ADVANCED MATERIALS INTERFACES
www.advmatinterfaces.de

From Amorphous Macroporous Film to 3D Crystalline Nanorod Architecture: A New Approach to Obtain High-Performance V_2O_5 Electrochromism

Zhongqiu Tong, Xiang Zhang, Haiming Lv, Na Li, Huiying Qu, Jiupeng Zhao, Yao Li, and Xiang-Yang Liu**

A 3D crystalline V_2O_5 nanorod architecture on indium tin oxide substrates is prepared by simple annealing treatment of a colloidal crystal-assisted electrodeposited amorphous three-dimensionally ordered macroporous film at a low temperature of 350 °C. The crystalline nanorods exhibit a low length/diameter ratio with the typical width range of 80–180 nm, length range of 190–500 nm, and thickness of 30–50 nm. Colloidal sphere-assisted heterogeneous nucleation during electrodeposition and the anisotropic bonding of the V_2O_5-layered structure are two important factors for the morphological changes. Because of the large surface area, short lithium ion diffusion distance, and good electrolyte penetration, the 3D crystalline V_2O_5 nanorod architecture exhibits a highly reversible Li-ion insertion/extraction process (columbic efficiency up to 96.9%) with a five-color-change electrochromic performance, good transmittance modulation, and acceptable response times (8.8 s for coloration and 9.3 s for bleaching), making it a promising film electrode for electrochromic devices.

1. Introduction

The reversible, persistent electrochromic (EC) change in color or optical parameters controlled by a temporarily applied electrical potential is attractive because of numerous potential applications in variable transmittance windows (smart windows), display devices, and controlled reflectance mirrors.[1–3] Transition metal oxides such as tungsten, vanadium, titanium, molybdenum, and nickel oxides are some of the well-known EC materials.[4–8] Among these oxides, V_2O_5 is of particular interest. As the only one oxide which can show both anodic and cathodic coloration, the reversible lithium ion insertion/extraction processes of V_2O_5 lead to not only reversible optical parameter changes but also multicolor changes for esthetics in the voltage range of ±1 V.[3,8–11] However, due to several disadvantages originating from its low electric conductivity (10^{-3}–10^{-2} S cm^{-1}), low Li^+ diffusion coefficient (10^{-13}–10^{-12} cm^2 s^{-1}), long lithium diffusion distance, and small surface area, the lithiation processes in conventional flat V_2O_5 film are rather slow, resulting in low coloration contrast, slow switching speed, and unstable cycling performance for electrochromism.[12–15] The remarkably improved Li-ion diffusion kinetics and enhanced EC performance observed for V_2O_5 nanostructures (as compared to bulk V_2O_5) have spurred increasing interest in the synthesis of V_2O_5 nanostructures with tunable dimensions.[9,15–17] Fabricating 3D nanoscale oxides with interconnected pore spaces has been explored to significantly improve the material performance through enhancing the surface area for redox reaction, the reduction in the required diffusion length, and the good electrolyte penetration from the interconnected voids.[9,14–17] In moving forward, when the nanoscale oxides are in forms of 1D nanostructures (e.g., nanowires, nanorods, nanoribbons, and nanotubes), the intrinsic advantages of these nanostructures for Li-ion diffusion kinetics, such as large surface area, facile strain relaxation, and efficient 1D electron transport, can further enhance the oxides' EC performance.[14–17]

One widely used method for fabricating 3D V_2O_5 films with 1D V_2O_5 nanowires or nanoribbons is a three-step process.[18–20] The 1D nanowires or nanoribbons are firstly prepared by hydrothermal or sol–gel syntheses, and then the 1D nanomaterials are integrated into porous sheets by a filtration process. Finally, the sheets are transferred to a transparent current collector (e.g., indium tin oxide (ITO), fluorine-doped tin oxide (FTO)) for subsequent test or usage. However, this multiple-step process is rather complex for the fabrication of the full EC device and usually leads to the filtered film that lacks mechanical integrity to some extent. By using the catalytic growth process[21] or vapor

Dr. Z. Q. Tong, Dr. X. Zhang,
Dr. H. M. Lv, Prof. Y. Li
Center for Composite Materials
Harbin Institute of Technology
Harbin 150001, China
E-mail: yaoli@hit.edu.cn
Dr. N. Li, Dr. H. Qu, Prof. J. Zhao
School of Chemical Engineering and Technology
Harbin Institute of Technology
Harbin 150001, China
Prof. X.-Y. Liu
Research Institute for Soft Matter and Biomimetics
College of Materials and Department of Physics
Xiamen University
Xiamen 361005, China
E-mail: Liuxy@xmu.edu.cn

DOI: 10.1002/admi.201500230

 © 2015 WILEY-VCH Verlag GmbH & Co. KGaA, Weinheim

transport method,[22] V_2O_5 nanowire arrays or porous film composed of V_2O_5 nanoribbons can be directly grown on the silicon substrates; however, the high synthesis temperature (above 600 °C) makes the transparent current collectors not suitable for being the alternative substrates. Takahashi et al. combines electrophoretic deposition with the use of a membrane template to directly obtain single-crystalline V_2O_5 nanorod array on ITO substrate, but its switching time is rather long even under a high polarization voltage of 3 V due to the sluggish kinetics of Li-ion insertion/extraction along the longitude direction caused by the long length of the nanorods (≈10 μm).[9,17,22,23] Thus, practical implementation of the 3D nanoscale V_2O_5 film on a transparent current collector for high-performance electrochromism still remains a challenge.

Here, we demonstrate a novel method for the first time to in situ fabricate a 3D V_2O_5 nanorod architecture on transparent current collector directly from a 3D ordered macroporous (3DOM) film simply by annealing at a low temperature of 350 °C. The mechanism of the morphological transformation is discussed and the effects of annealing temperature on the EC performance are investigated. The nanorods exhibit low length/diameter ratio and thin thickness. The remarkable 3D V_2O_5 nanorod architecture exhibits a multicolor EC performance with good transmittance modulation and acceptable response time, making it a promising film electrode for EC devices.

2. Results and Discussion

Our approach for the fabrication of the 3D V_2O_5 nanorod architecture involved two key steps. Firstly, anodic deposition of V_2O_5 into the polystyrene (PS) colloidal crystal templates was performed from a $VOSO_4$ solution to fabricate the 3DOM film (Figure S1a–c, Supporting Information). Subsequently, annealing treatment was used to transform the 3DOM structure to the aimed 3D nanorod architecture. **Figure 1** shows the top-view and cross-section scanning electron microscopy (SEM) images of the 3DOM V_2O_5 films subjected to annealing under different conditions. Digital photographs of these films are shown in Figure S2 (Supporting Information). Because the nanostructure was replicated from the colloidal crystal, the as-prepared film exhibited a honeycomb-like structure throughout their entire volume with a pore wall thickness of ≈18 nm (Figure 1a and Figure S1d, Supporting Information). Because of the shrinkage during annealing, the macroporous structure had deformed slightly. The film was greenish yellow, probably owing to the presence of V^{4+} ions.[19] This 3DOM nanostructure could withstand annealing temperatures of up to 250 °C for 4 h (Figure 1b). Interesting morphological changes were noticed after the film was annealed at 300 °C for 4 h (Figure 1c). At this temperature, the 3DOM film disintegrated completely, resulting in the formation of curving platelets. This morphological change indicated that a phase transformation as well as crystal growth occurred during the annealing process at this temperature. Novel V_2O_5 nanorods formed after being annealed at 350 °C for 4 h (Figure 1d). The cross-section SEM image of 350 °C–4 h film exhibited that the morphological changes not only occurred on the film surface but also across the whole gradient direction, resulting in the formation of 3D V_2O_5 nanorod architecture with intercontinuous voids (Figure 1e). Such intercontinuous voids can provide good electrolyte penetration for facile redox reactions when the film was used as the EC film electrodes. The thickness of the film was ≈860 nm. Low-magnification SEM image taken from the film indicated that all the 3DOM structures were morphologically transformed to the nanorods (Figure S3, Supporting Information). High-magnification SEM image showed that the surfaces of these nanorods were rough (Figure S4a, Supporting Information). The typical width and the length of the nanorods were 20–100 and 200–400 nm, respectively. Bright-field transmission electron microscopy (TEM) image showed that these nanorods were rather uniform and selected-area electron

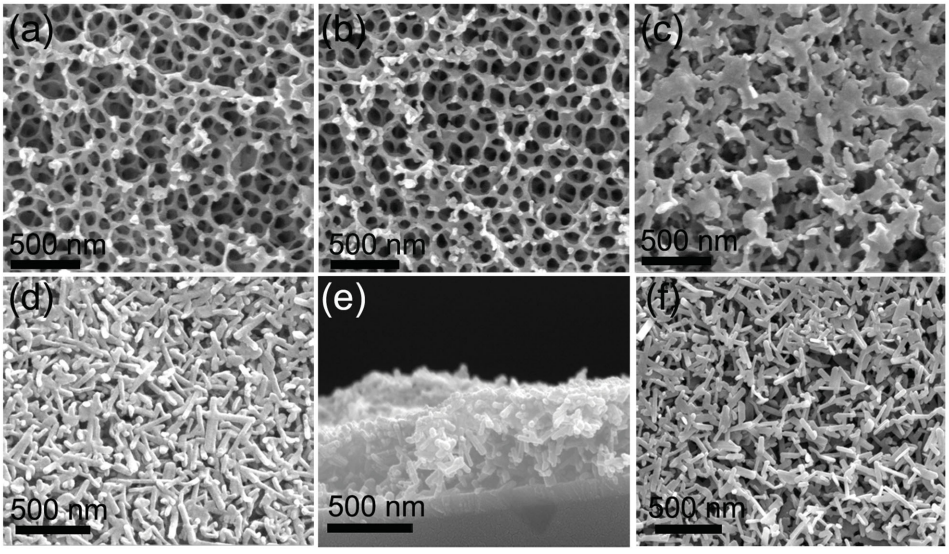

Figure 1. SEM images of the 3DOM V_2O_5 films annealed under different conditions: a) as-prepared, b) 250 °C for 4 h, c) 300 °C for 4 h, d, e) 350 °C for 4 h, and f) 350 °C for 7 h.

© 2015 WILEY-VCH Verlag GmbH & Co. KGaA, Weinheim

diffraction (SAED) pattern taken from these nanorods showed scattered diffraction pots overlapping on the amorphous ring (Figure S4b,c, Supporting Information). This indicated these nanorods were mixed with crystallites and amorphous parts. To further investigate the microstructure of these nanorods, a higher magnification bright-field TEM was taken. As shown in Figure S4d (Supporting Information), it can be found that some of these nanorods showed a core/shell structure. Rod-like inner cores were surrounded by shells with irregular shape. One rod-like inner core showed a diameter of 16.2 nm. In the following research, the rod-like inner cores were proved to be orthorhombic V_2O_5, while the outer irregular shells were amorphous V_2O_5. After annealed at 350 °C for 7 h, V_2O_5 nanorods with a rectangular cross-section and nearly round tips were achieved, and showed a low length/diameter ratio with the typical width range of 80–180 nm, length range of 190–500 nm, and thickness range of 30–50 nm (Figure 1f and Figure S5a, Supporting Information). The smooth surface was clearly dominated by a particular type of crystal facets, which can be proved by the high-resolution TEM (HRTEM) examination result of one nanorod. Clearly lattice-resolved HRTEM images and the indexed SAED pattern revealed the nanorod morphology of a single orthorhombic V_2O_5 microcrystal (Figure S5c,d, Supporting Information). The observed spacing between the lattice fringes can be assigned to the (401) planes of orthorhombic V_2O_5 phase. In addition, as shown in Figure S6 (Supporting Information), the prolonged annealing time at 350 °C had no obvious influence on the morphology. The 350 °C 7 h film still exhibited a 3D V_2O_5 nanorod architecture, but the size of intercontinuous voids significantly increased. On the other hand, in the case of the V_2O_5 film electrodeposited directly on an ITO-coated glass substrate, no morphological changes were noticed after the film had been annealed at 350 °C for 7 h (Figure S7a,b, Supporting Information). In addition, even in the case of a 3DOM V_2O_5 film prepared by the spin coating of a V_2O_5 gel, no morphological changes were observed after the film was annealed at the same temperature and time (Figure S7c, Supporting Information). Thus, we could conclude that colloidal templates play an important role with regard to crystal nucleation during electrodeposition as well as with respect to crystal growth during the subsequent annealing process.

X-ray diffraction (XRD) examination was used to investigate the phase changes of 3DOM films during the annealing processes (**Figure 2**a). The fact that the XRD pattern of the as-prepared 3DOM film contained only a single broad diffraction peak at ≈21.6° and no diffractions related to V_2O_{5-x} or $V_2O_{5-x}\cdot nH_2O$ indicated that the film was amorphous; the other peaks observed were related to the ITO layer. After the film was annealed at 250 °C for 4 h, the XRD pattern did not change, indicating that either no crystal growth occurred or the amount of new formed crystallites was too low to be detected during the XRD measurements. In keeping with the SEM observations, annealing treatment at 300 °C for 4 h resulted in the appearance of crystals, leading to structural disintegration. As a result, an XRD peak was noticed at 21.6°, which corresponded to the (001) plane of orthorhombic V_2O_5 (JCPDS 41-1426). When annealing was performed at 350 °C for 4 h, the broad diffraction peak was still observed, indicating that amorphous V_2O_5 remained in the film. Further, after the film had been annealed

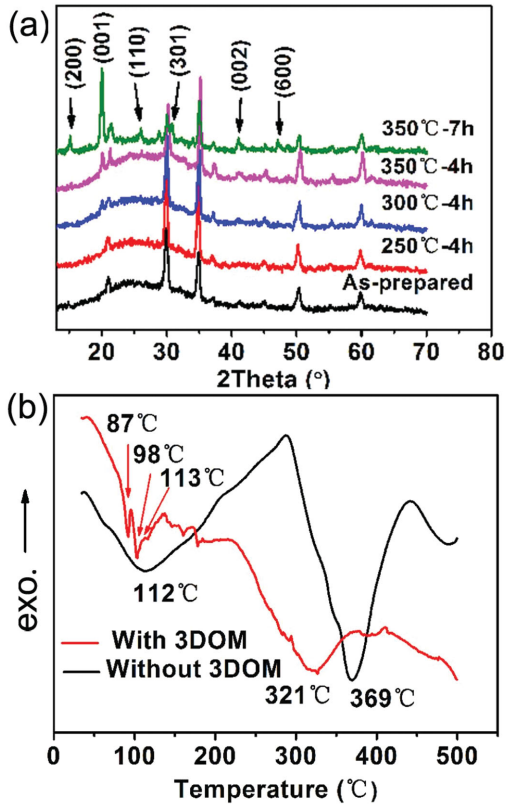

Figure 2. a) XRD patterns of the 3DOM V_2O_5 films annealed at different conditions. b) DSC curves of the 3DOM film and the dense film in air; the heating rate was 5 °C min^{-1}.

at 350 °C for 7 h, the amorphous phase-related diffraction peak disappeared and the film became completely crystallized, exhibiting a purely orthorhombic V_2O_5 phase with good crystallinity, as can be seen in the XRD pattern. This result was consistent with the HRTEM, SAED, and SEM examination results of the 350 °C–7 h film.

Differential scanning calorimetry (DSC) was employed to further analyze the crystallization of the 3DOM films during annealing (Figure 2b). The DSC result for the dense film was also shown for comparison. Both the 3DOM film and the dense film exhibited thermodynamic characteristics similar to that of a $V_2O_5\cdot nH_2O$ xerogel;[24,25] this suggested that two films were consisted of hydrated vanadium oxide. In the case of the dense film, the endothermic peak at ≈112 °C was probably attributable to the generation of $V_2O_5\cdot 0.6H_2O$, while the endothermic peak at ≈369 °C indicated the successful dehydration of $V_2O_5\cdot nH_2O$ and then crystallization to V_2O_5.[24,25] As to the 3DOM film, the broad endothermic band between 84 and 136 °C was overlapped by three endothermic peaks, which was located at 87, 98, and 113 °C. The previous two peaks were attributable to the absorbed organic molecules (dimethylformamide (DMF), toluene, and tetrahydrofuran (THF)) in the films, and the remaining peak could be probably attributable to the generation of $V_2O_5\cdot 0.6H_2O$. However, in 3DOM materials, the endothermic peaks corresponding to the phase-transformation processes were shifted to lower temperatures, indicating that the colloidal template was favorable to obtain crystallized

 © 2015 WILEY-VCH Verlag GmbH & Co. KGaA, Weinheim

V_2O_5 materials, and the full crystallization temperature was decreased to a low temperature of 321 °C.

Meanwhile, X-ray photoelectron spectroscopy (XPS) was used to probe the electronic structures of chemical bonds present in the films before and after annealing. The V $2p_{3/2}$ core peak spectra for the as-prepared 3DOM film (Figure S8a, Supporting Information) was composed of two components, which were located at 517.7 and 516.4 eV, as shown in the fitting data. These two binding energy values can be associated with two formal oxidation degrees, +5 and +4.[26–28] The V^{4+}/V^{5+} ratio was determined to be 0.19 from the area ratio of the fitted curves of the V $2p_{3/2}$ (V^{5+}) and V $2p_{3/2}$ (V^{4+}) spectra. The V^{4+} ions in the as-prepared film may be attributed to the VO^{2+} ions in the solution. When the process of VO^{2+} anodic oxidation and then deposition on ITO substrate occurs (as shown in Equations (3) and (4) in the Experimental Section), the codeposition of the unreacted VO^{2+} ions in the solution results in the presence of V^{4+} ions in the as-prepared film. The existence of V^{4+} ions in the as-prepared 3DOM film corroborated its greenish yellow color (Figure S2, Supporting Information). After being annealed at 350 °C for 7 h, the introduction of oxygen led to the oxidation and crystallization of the film. Therefore, vanadium ions were present only in the highest oxidation state (i.e., as V^{5+}) (Figure S8b, Supporting Information). Because the vanadium ions had a valence state of +5, the annealed vanadium oxide film was yellow.

Based on the above results, it can be concluded that the colloidal PS sphere template played a vital role in the morphological transformation from 3DOM structure to a 3D V_2O_5 nanorod architecture after annealing treatment. To further elucidate the effect of the colloidal template on crystal nucleation and the subsequent crystal growth process, TEM, HRTEM, and SAED examinations were performed to investigate the crystalline changes of the 3DOM V_2O_5 films during annealing. As shown in **Figure 3**a, the as-prepared 3DOM V_2O_5 films contained a certain number of crystal nuclei. The size of these crystal nuclei was ⩾1–2 nm. The observed lattice spacing was »0.236 nm, which corresponded to the distance between the (005) crystal planes of $V_2O_5 \cdot 1.6H_2O$ (JCPDS No. 40-1296). In XRD examination, the reason for the absence of diffraction peaks belonging to $V_2O_5 \cdot 1.6H_2O$ phase may be due to the amount of these crystal nuclei which was too small to be detected. The distribution of these crystal nuclei was worth noting. The nuclei were located near the wall surfaces, with their number density decreasing significantly as one moved away from the wall surfaces. We believe this phenomenon was

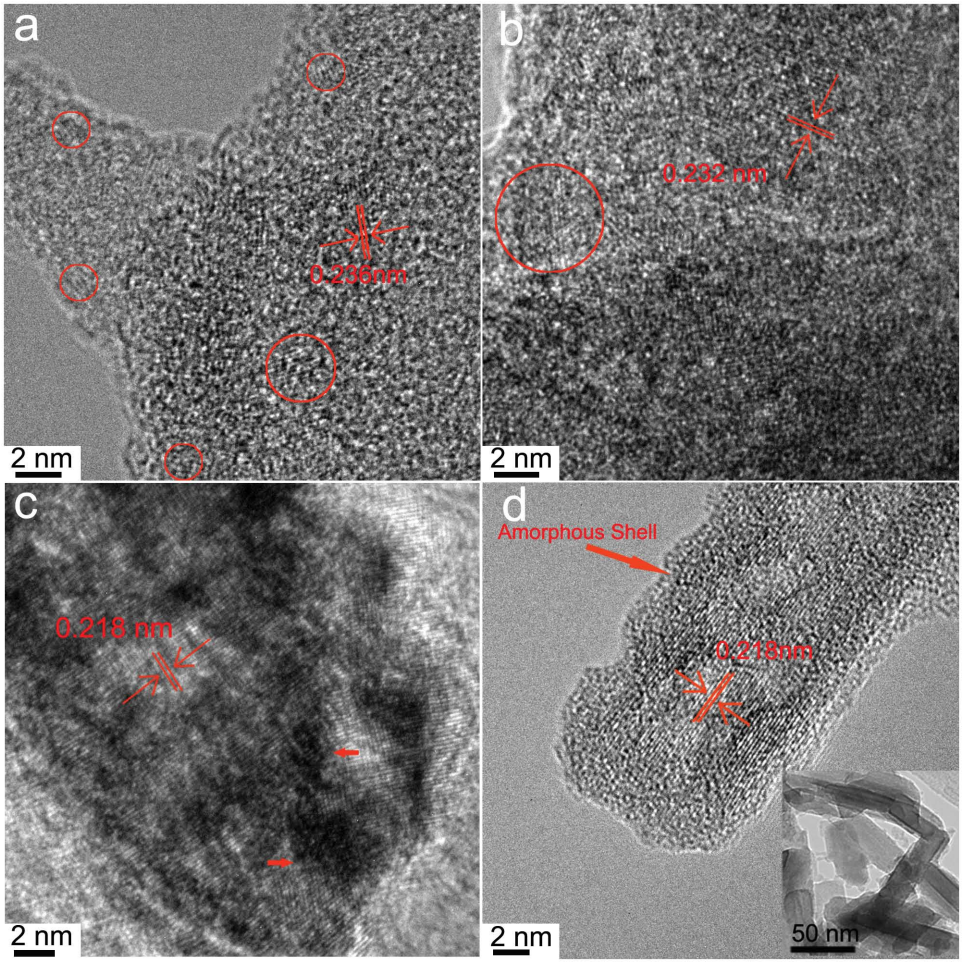

Figure 3. HRTEM images of the 3DOM V_2O_5 films annealed at different temperatures: a) as-prepared, b) 250 °C for 4 h, c) 300 °C for 4 h, and d) 350 °C for 4 h. The inset image in (d) is a TEM image of the nanorods.

© 2015 WILEY-VCH Verlag GmbH & Co. KGaA, Weinheim

caused by the colloidal PS crystals. The PS spheres accumulated charge on their surfaces (their zeta potential was approximately −21.2 mV). Thus, the electric field resulting from these surface charges rearranged the atoms during the electrodeposition process, leading to the appearance of crystal nuclei near the surfaces of the 3DOM skeletal walls. In addition, the rough surfaces of the PS sphere (Figure S1c, Supporting Information) also provided low-energy sites for heterogeneous nucleation during the electrodeposition process. With an increase in the annealing temperature to 250 °C (for 4 h), the nuclei grew into nanocrystallites (Figure 3b). The size of these nanocrystallites was ~5–10 nm. Further, the observed interlayer spacing was 0.232 nm; this value still corresponded to the distance between the (005) crystal planes of $V_2O_5 \cdot 1.6H_2O$. These nanocrystallites were small and distributed on the wall surfaces. Thus, it could be concluded that crystal growth did not cause the collapse of the 3DOM structure. Nanorods were observed when the films were annealed at 300 °C for 4 h (Figure 3c and Figure S9, Supporting Information). The observed lattice spacing was ⩾0.218 nm, which corresponded to the distance between the (002) crystal planes of orthorhombic V_2O_5. The formation of the V_2O_5 nanorods could be attributed to the anisotropic bonding of the layered V_2O_5 structure. In orthorhombic V_2O_5, weakly bonded basal {001} planes lead to the surface energy being ~0.7 J m^{-2}, resulting in the <010> direction being the fast-growth one and the <001> direction being the slow-growth one.[21,29] The amorphous phase is in metastable equilibrium and, under thermal activation, can be induced to be crystallized. At the boundary between the crystalline and amorphous V_2O_5 phases, the crystallite surfaces provided low-energy sites for the atoms of the amorphous phase to rearrange into a crystal lattice in the manner of the parent crystallites, instead of creating new grain boundaries. In addition, atoms were also rearranged at the grain boundaries between neighboring crystallites (as pointed out by the red arrows). This type of atomic rearrangement at the grain boundaries led to the larger crystallites coalescing with the smaller ones during the annealing process. In addition, the length of the growing nanorods was greater than 45 nm (Figure S10, Supporting Information). Crystallites this long can cause the collapse of the 3DOM structure. After the films had been annealed at 350 °C for 4 h, distinct nanorods were observed (Figure 3d). Because the annealing time was not long enough for all the amorphous V_2O_5 atoms to rearrange into crystallites, an amorphous V_2O_5 phase remained, covering the crystalline nanorods, and then leading to the formation of the some crystalline/amorphous core/shell V_2O_5 nanorods (see the insets of Figure 3d). With an increase in the annealing time to 7 h (for an annealing temperature of 350 °C), the nanorods became fully crystallized and thus exhibited smooth surfaces.

PS spheres with positively charged surfaces (zeta potential of approximately +25.6 mV) were used to investigate the effects of the charge type on the morphological changes induced during the annealing process (Figure S7d, Supporting Information). When the film was annealed at 350 °C for 4 h, only curving platelets were formed, and nanorods were not noticed. This indicated that a negative surface charge was better suited for growing V_2O_5 nanorods. The reasons for this may be rooted in the nature of the electrodeposition reactions. Before V_2O_5 can be deposited (Equation (2)), the oxidation of VO^{2+} ions to $H_2V_{10}O_{28}^{4-}$ (Equation (1)) is necessary. A negative surface charge is preferred because of the electrostatic attraction between the negative surface charge and the positive VO^{2+} ions, which causes the $V_2O_5 \cdot 1.6H_2O$ crystal nuclei to come very close to the surfaces of the PS spheres (Figure 3a).

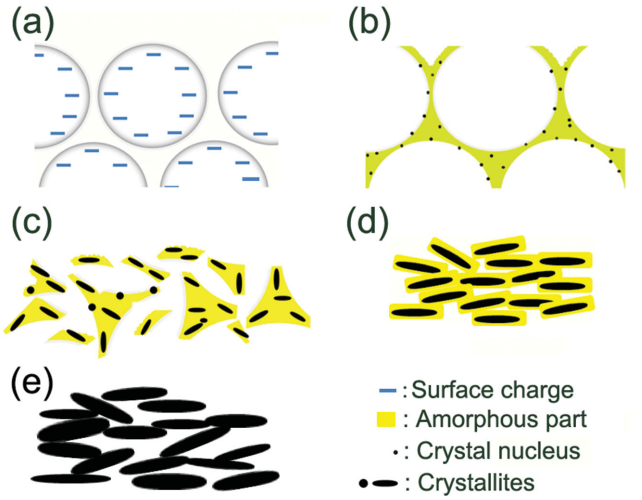

Figure 4. Schematic of morphological transformation in the 3DOM film during annealing treatment. a) PS spheres with negative surface charges. b) An as-prepared amorphous 3DOM film with crystal nuclei on its wall surfaces. c) Structural disintegration of the 3DOM V_2O_5 film by the grown nanorods when the size of the nanorods becomes greater than the thickness of the 3DOM walls. d) Coalescing of the nanocrystallites and induced crystallization between the V_2O_5 nanocrystallites and the amorphous V_2O_5 produces crystalline/amorphous core/shell V_2O_5 nanorods. e) Fully crystallized V_2O_5 nanorods are formed when the annealed time is long enough.

On the basis of the above-mentioned facts, a model for the synthesis of crystalline nanorods from the amorphous 3DOM structure is proposed (**Figure 4**). In this model, PS sphere-assisted heterogeneous nucleation during electrodeposition and the anisotropic bonding of the V_2O_5-layered structure are the two most important factors. The surface charge and roughness of the colloidal spheres result in heterogeneous nucleation occurring on the surfaces of the colloidal spheres during electrodeposition (Figure 4a). After the removal of the colloidal spheres, the crystal nuclei sit on the surfaces of the 3DOM walls (Figure 4b). Due to the anisotropic bonding of V_2O_5, the layered structure with a very low surface energy along the basal {001} planes makes the <010> being the fast-growth direction, resulting in the formation of 1D crystals. Further, under thermal activation at the proper temperature, dehydration, the coalescence of nanocrystallites, and induced crystallization between nanocrystalline V_2O_5 and amorphous V_2O_5 cause the growth of nanorods in the 3DOM amorphous walls. This crystal growth process leads to morphological disintegration when the size of nanorods becomes equal to the thickness of the 3DOM walls (Figure 4c). When the annealing time is increased, the continuous coalescence of the nanocrystallites occurs, and the induced crystallization between nanocrystalline V_2O_5 and amorphous vanadia results in nanorods with a crystalline/amorphous core/shell structure or fully crystallized nanorods (Figure 4d and Figure 4e, Supporting Information).

© 2015 WILEY-VCH Verlag GmbH & Co. KGaA, Weinheim

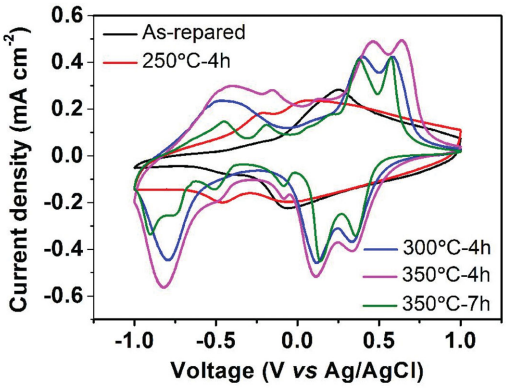

Figure 5. CV curves of the 3DOM V_2O_5 films annealed under different conditions. Curves were obtained at 10 mV s^{-1} in 1 M $LiClO_4$/PC as electrolyte for potentials ranging from –1 to +1 V (vs Ag/AgCl).

Cyclic voltammetry (CV) measurements were performed to evaluate the electrochemical behaviors of the annealed films. **Figure 5** presents the CV curves of three 3DOM films and the dense V_2O_5 film obtained at a scan rate of 5 mV s^{-1} using 1 M $LiClO_4$ propylene carbonate electrolyte and a potential window of ±1 V. The shapes of the CV curves varied with the annealing conditions, indicating that the annealing temperature and time had a significant influence on the electrochemical properties of the V_2O_5 films. For the as-prepared and 250 °C–4 h films, the absence of phase transformation redox peaks indicated the amorphous nature of the samples,[15,21,30,31] which was consistent with XRD and TEM results. After being annealed at 300 °C for 4 h, CV curve of 300 °C–4 h film showed typical electrochemical behaviors of orthorhombic V_2O_5 phase, according to the literatures.[15,21,30,31] When the annealing temperature increased to 350 °C, the number of redox reaction peaks further increased with the increase of annealing time; this phenomenon confirmed a further increase in the crystallinity of the films.

In situ visible and near-infrared (NIR) transmittance measurements were used to investigate the effects of the annealing conditions on the EC performance. Transmittance modulation (ΔT) of the films and the transmittance spectra were recorded every 0.5 V. As shown in **Figure 6**, upon applying external potential changes, all the vanadia films exhibited obvious transmittance and color changes. The ΔT values obtained at two typical wavelengths of 460 and 1000 nm were listed in **Table 1**. Maximum ΔT of 38.48% at 460 nm was found in 350 °C–4 h film, followed by 34.01% in the as-prepared film. The 300 °C–4 h and 350 °C–7 h films showed moderate ΔT, while the 250 °C–4 h film exhibited a minimum ΔT at this wavelength (18.49%). At NIR wavelength of 1000 nm, the 350 °C–7 h film showed a maximum ΔT (36.69%) and the minimum ΔT of 16.41% was found in the as-prepared film. Table S1 (Supporting Information) shows the comparison of the EC performance of two 3D nanorod architectures (350 °C–4 h film and 350 °C–7 h film) with that of vanadia dense films and vandia nanostructures. As exhibited in the table, it can be found that the two 3D nanorod architectures exhibit higher transmittance modulation than that of many other vanadia nanostructures. For all the samples, the transmittance spectra showed similar shape in the visible range under +1 V. An anodic potential of +1 V caused Li-ion extraction from vanadia films, giving rise to high transmission above 550 nm with substantial absorption in the 400–550 nm range. The different transmittance values at specific wavelength made these films present slight color difference from yellow to

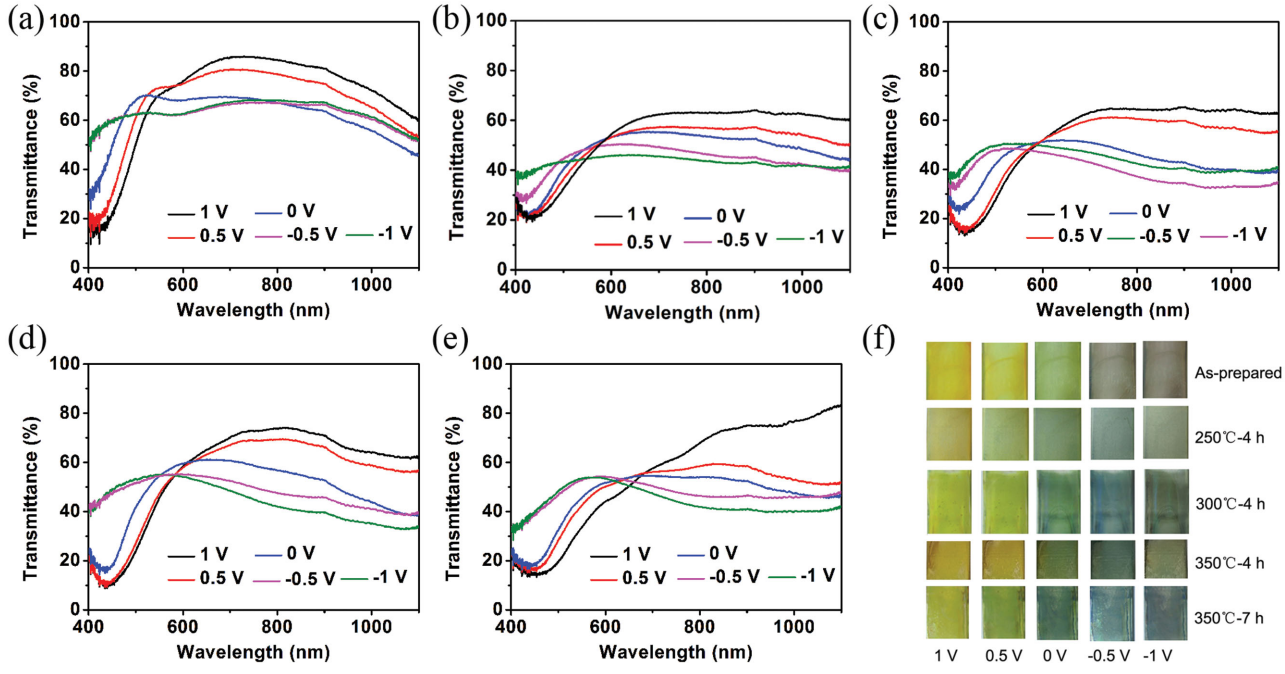

Figure 6. Transmittance contrast of the 3DOM V_2O_5 films annealed under different conditions: a) as-prepared, b) 250 °C for 4 h, c) 300 °C for 4 h, d,e) 350 °C for 4 h, and f) 350 °C for 7 h. f) Electrochromic digital photographs of the corresponding films under different potentials.

© 2015 WILEY-VCH Verlag GmbH & Co. KGaA, Weinheim

Table 1. Electrochromic characteristics of the 3DOM V_2O_5 films annealed at different conditions.

Sample	Coloration contrast [%]		Switching time [s]		Integrated charge [C cm^{-2}]		Columbic efficiency [%]
	At 460 nm	At 1000 nm	Coloration	Bleaching	Coloration	Bleaching	
As-prepared	34.01	16.41	2.3	4.5	0.0159	0.0133	83.6
250 °C–4 h	18.49	20.89	1.7	4.0	0.0194	0.0171	88.1
300 °C–4 h	29.85	31.62	5.7	7.1	0.0316	0.0279	88.3
350 °C–4 h	38.48	28.94	6.5	8.0	0.0426	0.0420	98.5
350 °C–7 h	27.43	36.69	8.8	9.3	0.0326	0.0316	96.9

yellow-green (Figure 6f). However, apparent color difference was found when these films were under –1 V. As to the as-prepared and 250 °C–4 h films, charge insertion under a cathodic potential of –1 V caused a fairly homogeneous transmission across the entire visible spectral range, resulting in a black coloration. For the remaining samples, the transmission in visible range was heterogeneous and with a peak between 450 and 600 nm. The different position of this transmission peak made these three films show different colors, i.e., dark green (300 °C–4 h film), olive (350 °C–4 h film), and Prussian blue (350 °C–7 h film). Usually, the valence of vanadium ion in vanadia films can be changed from +5 to +3 between –1 V and +1 V (vs Ag/AgCl),[26] indicating different voltages could lead to different amount mixture of V^{5+}, V^{4+}, and V^{3+} ions, resulting in more than two color changes in the voltage window of ±1 V.[32] Digital photos of the films at 0.5 V, 0 V, and –0.5 V were also exhibited in Figure 6f. It is interesting to find that the 350 °C–7 h film showed three more distinctive colors (yellow-green at 0.5 V, dark slate gray at 0 V, and steel blue at -0.5 V), while the as-prepared film presented only one more color (green at 0 V). The remaining vanadia films showed two more colors, i.e., 350 °C–4 h film (green at 0 V and blue at -0.5 V), 300 °C–4 h film (dark green at 0 V and blue at –0.5 V), and 250 °C–4 h film (green at 0 V and prussian blue at –0.5 V). Thus, it can be concluded that the 350 °C–7 h film showed maximum number of five-color changes in the voltage range of ±1 V (yellow, yellow-green, dark slate gray, steel blue, and prussian blue), while the as-prepared film presented minimum number of three-color changes (yellow, green, and black). Cycling stability is another important aspect for EC materials. The transmittance modulations of the films annealed at different conditions after the 100th cycle are shown in Figure S11 (Supporting Information). As shown in the figure, all vanadia films showed good cycling stability. After 100 cycles, only slight transmittance modulation degradation was found. Large surface area and reasonable Li-ion diffusion distance of these films are the two important factors for the high cycling stability.

A third important aspect of electrochromism is the temporal response under alternating voltages. Switching behavior was analyzed by monitoring the transmittance at a wavelength of 460 nm under the application of a square wave voltage between +1 V and –1 V. The 3DOM films (the as-prepared film and 250 °C–4 h film) exhibited sharp and distinct transitions between coloration and bleaching state, while the films with morphological changes (300 °C–4 h film, 350 °C–4 h film, and 350 °C–7 h film) showed gradual transitions (**Figure 7**). This phenomenon clearly indicates that 3DOM films had much faster switching times than the morphologically changed films. The switching time, defined as 90% of the total transmittance change, was summarized in Table 1. As shown in the table, the 3DOM films showed high switching speed. The corresponding switching time was 2.3 s for coloration and 4.5 s for bleaching

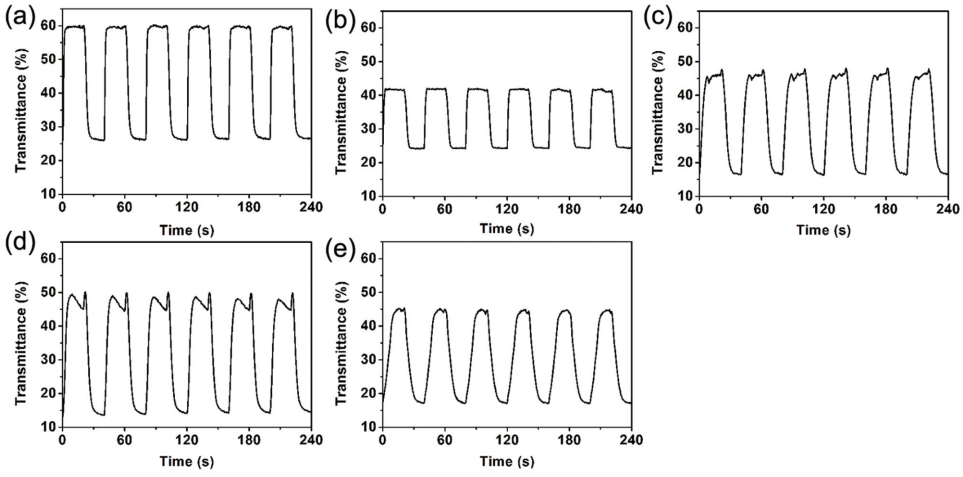

Figure 7. Transmittance–time response curves of the 3DOM V_2O_5 films annealed under different conditions: a) as-prepared, b) 250 °C for 4 h, c) 300 °C for 4 h, d) 350 °C for 4 h, and e) 350 °C for 7 h. The monitored wavelength was 460 nm and voltages were alternated between +1 V and –1 V.

 © 2015 WILEY-VCH Verlag GmbH & Co. KGaA, Weinheim

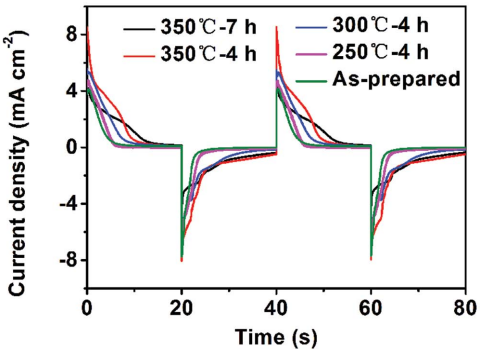

Figure 8. Current–time response curves of the 3DOM V_2O_5 films annealed under different conditions. Voltages were alternated between +1 V and −1 V.

in the as-prepared film, and 1.7 s for coloration and 4.0 s for bleaching in the 250 °C–4 h film. With the increase of the annealing temperature and time, the switching time for both coloration and bleaching prolonged. For the 350 °C–7 h film, the switching time of coloration and bleaching was prolonged to 8.8 and 9.3 s, respectively. However, these two switching values were still acceptable when the 350 °C–7 h film was used for the fabrication of EC device.[3] Xiong et al. reported the color-switching time of a filtered V_2O_5 nanowire film to be ⩾12.5 s for coloration under –1.5 V and ⩾10.4 s for bleaching under +2.5 V when 90% transmittance change was defined.[19] Takahashi et al. reported that a 30% transmittance modulation at 700 nm took 50 s for a V_2O_5 nanorod array when 3.0 V was applied, and 300 s was required for a sol-gel V_2O_5 film.[23] The main reason for the prolonged switching times in morphologically changed films was the increased lithium diffusion distance.[9] In the 3DOM films, the lithium diffusion distance was half the thickness of 3DOM walls (9 nm); however, this value increased to 15–25 nm (half the thickness of nanorods) in the 350 °C–7 h film. The increased lithium diffusion distance indicated the time required to achieve satisfactory color saturation switching increased. **Figure 8** showed the current–time response curves of the vanadia films during the switching response measurement. Consistent with the transmittance–time response curves, currents of the 3DOM films reached the equilibrium state faster than those of morphologically changed films. However, by calculating the integrated charge during the coloration and bleaching processes, it can be found that both V_2O_5 films with 3D V_2O_5 nanorod architecture showed high columbic efficiency (98.5% in 350 °C–4 h film and 96.9% in 350 °C–7 h film), as shown in Table 1. High columbic efficiency indicated the redox reactions during EC processes were highly reversible, which was beneficial to the cycling performance. In contrast, the as-prepared film presented minimum columbic efficiency of 83.6%.

Optical density (OD) and coloration efficiency (CE) are two important parameters for the evaluation of an EC material's optical modulation ability.[1-3] OD and CE can be defined as[1–3]

$$\mathrm{OD} = \log(T_{b\lambda} / T_{c\lambda}) \quad (1)$$

$$\mathrm{CE} = \mathrm{OD}/Q_{in} \quad (2)$$

where $T_{b\lambda}$ and $T_{c\lambda}$ represent the transmittance of the bleached and colored samples, respectively. Q_{in} corresponds the injected/ejected charge density per unit area. Obviously, CE presents the ability of optical modulation during the coloration-bleaching process under the considering of energy consumption. Figure S12a,b (Supporting Information) shows the OD and CE values of the vanadia films annealed at different conditions. As shown in Figure S12a (Supporting Information), 350 °C–4 h film exhibited the highest OD in the whole spectrum range, indicating its good optical modulation ability. As shown in Figure S12b (Supporting Information), the as-prepared film showed the highest CE values in visible spectrum range of 400–500 nm. The average CE value in this range reached 25.2 $cm^2\ C^{-1}$. The reason for the high CE value of as-prepared film in this spectrum range can be explained from two aspects. Firstly, the high transmittance modulation in this range ensured it high OD value. Secondly, as shown in the CV (Figure 5) curves and current–time response curve (Figure 8), the smallest CV curve area and integrated charge indicated the number of intercalated Li-ions was least among the vanadia films. Thus, by Equations (1) and (2), it is reasonable to find the as-prepared film showed high CE value in this spectrum range. As for the two films with 3D V_2O_5 nanorod architecture (350 °C–4 h film and 350 °C–7 h film), although their transmittance modulations in the whole spectrum range were relatively high, the large number of intercalated Li-ions made their CE values very low. The average CE values of 350 °C–4 h film and 350 °C–7 h film in whole spectrum range were only 8.9 and 7.1 $cm^2\ C^{-1}$, respectively. However, a low CE value also meant that a large amount of Li-ions was stored in the V_2O_5 films during the redox processes. In other words, such V_2O_5 films have good charge storage ability and can be used as binder-free film electrode for Li-ion batteries or electrochemical capacitors.

3. Conclusion

In conclusion, we described the fabrication of the 3D V_2O_5 nanorod architecture on ITO substrate by simple annealing treatment of the 3DOM film at a low temperature of 350 °C. The V_2O_5 nanorods shared a low length/diameter ratio and thin thickness. Such 3D V_2O_5 nanorod architectures have been investigated to be desirable for the EC device with multicolor changes, high optical modulation, and acceptable switching times. Furthermore, the results of this study can act as a guide for investigating the morphological changes and nucleation processes in porous materials prepared from templates. The highly reversible redox reactions will also make them useful in the applications of binder-free lithium ion batteries and electrochemical capacitors, which are the main aspects of future works.

4. Experimental Section

Fabrication of 3D V_2O_5 Nanorod Architecture: Colloidal polystyrene (PS) spheres (diameter of 250 nm) were synthesized through an emulsifier-free emulsion polymerization technique. Templates consisting of the colloidal PS crystals were grown using a controlled vertical drying method.[26] ITO-coated glass was used for the substrates

© 2015 WILEY-VCH Verlag GmbH & Co. KGaA, Weinheim

(⩾9 Ω cm^{-2}, 1 cm × 4 cm), which were cleaned ultrasonically for 20 min each in acetone, methanol, and distilled water. The cleaned substrates were then placed in cylindrical vessels. A suspension of the PS spheres, which had been diluted to 0.5 wt%, was added to the glass vessels. The vessels were then heated in an incubator at 60 °C.

The anodic deposition of V_2O_5 on the colloidal PS crystals was performed at a constant voltage of 2 V (vs Ag/AgCl) using a 1:1 mixture (volume ratio) of distilled water and ethanol containing 0.25 M $VOSO_4{\cdot}5H_2O$ as the electrolyte; a piece of Pt foil was used as the counter electrode. The pH of the electrolyte was adjusted to 2.7 using NaOH. The electrodeposition time was 32 s. The oxidation of VO^{2+} and the deposition of V_2O_5 occurred through the following reactions when $2.4 < pH < 2.7$[33]

$$10VO^{2+} + 18H_2O \rightarrow H_2V_{10}O_{28}^{4-} + 34H^+ + 10e^- \quad (3)$$

$$H_2V_{10}O_{28}^{4-} + 4H^+ \rightarrow 5V_2O_5 + 3H_2O \quad (4)$$

After the deposition of V_2O_5, the samples were immersed in a 1:1 mixture (volume ratio) of dimethylformamide (DMF) and toluene for 24 h to remove the PS templates, and then washed with tetrahydrofuran (THF). Finally, the as-prepared films were dried at 100 °C for 4 h (marked as as-prepared film) and annealed in air at one of the following temperatures for 4 h at a heating rate of 1 °C min^{-1}: 250, 300, or 350 °C (marked as 250 °C–4 h film, 300 °C–4 h film, and 350 °C–4 h film, respectively). Completely crystallized V_2O_5 film was formed after being annealed at 350 °C for 7 h (marked as 350 °C–7 h film). Further, a V_2O_5 film was directly deposited on an ITO-coated glass substrate without using the colloidal crystal template and then annealed for comparison; this film is referred to as the dense film.

To investigate the effects of electrodeposition on the morphological transformation of the 3DOM V_2O_5 films, a 3DOM V_2O_5 film was prepared using a V_2O_5 sol and annealed subsequently. First, a V_2O_5 sol was prepared by the quenching method. V_2O_5 powder (99.9%) was heated at 850 °C in a crucible until it melted. The melt was then quickly poured into deionized water at room temperature. After vigorous stirring for 1 d, a homogeneous V_2O_5 sol was obtained, whose concentration was ⩾0.02 M. The sol was dropped on colloidal PS crystals, and the crystals were spun. The spinning rate was 1000 rpm, and the spinning time was 30 s. PS spheres were also removed by DMF, toluene, and THF.

Characterization of Synthesized Films: The zeta potential of the PS spheres was measured with a Zetasizer Nano Series 90 system at 25 °C using a DTS 1060C disposable capillary cell (Malvern Instruments). The morphologies of the V_2O_5 films were characterized using scanning electron microscopy (SEM, FEI Helios Nanolab 600i). The crystalline structures of the V_2O_5 films were investigated using a rotation-anode X-ray diffractometer (Rigaku D/Max-γb) with a graphite monochromatized Cu Kα radiation (0.15418 nm) source as well as a high-resolution transmission electron microscopy (HRTEM, FEI Tecnai G2F30, 300 kV). A differential scanning calorimetry (DSC) system (Netzsch, STA 449C) was used to study the decomposition of the 3DOM structure and the crystal growth process. The Raman spectra of the films were recorded with a spectrophotometer (JY Co., LABRAM-HR) with an operating wavelength of 613 nm. X-ray photoelectron spectroscopy (XPS) was performed with a PHI 5700 ESCA system using Al Kα radiation (1486.6 eV).

EC Measurements: All the electrochemical measurements were performed with a CHI660C workstation. The organic electrolyte used was a 1 M solution of $LiClO_4$ in propylene carbonate. The ITO-coated glass substrates with V_2O_5 films were formed acted as the working electrodes, while a piece of Pt foil served as the counter electrode and an Ag/AgCl electrode was used as the reference electrode. Cyclic voltammetry (CV) measurements were performed at scanning rates of 10 mV s^{-1} for voltages of –1 V to +1 V.

In situ visible and near-infrared (NIR) EC measurements were performed using a laboratory-built experimental apparatus (same setup as that used in ref.[26] in combination with a CHI 660C electrochemical workstation (Shanghai Chenhua Instrument Co. Ltd.). The experimental apparatus was sealed in an Ar-filled glove box (Vigor Glove Box from Suzhou, China) before testing. One side of the apparatus was connected to a white lamp (DT-mini-2-GS, Ocean Optics) by an optical fiber; the other side was connected to an optical spectrometer (MAYA 2000-Pro, Ocean Optics). The V_2O_5 film, a Pt wire, and an Ag/AgCl electrode were used as the working electrode, counter electrode, and reference electrode, respectively. The transmittance of the ITO-coated glass substrate in the electrolyte was considered to be 100% and was used as the reference. Before investigating of the EC performance, all the vanadia films have been activated by CV at 0.5 mV s^{-1} for three circles, and then electrochemically polarized at +1 V for 3000 s for removal of all the intercalated Li-ions by chronoamperometry.

Supporting Information

Supporting Information is available from the Wiley Online Library or from the author.

Acknowledgements

This work was supported by the National Natural Science Foundation of China (Nos. 51010005, 91216123, and 51174063), Natural Science Funds for Distinguished Young Scholar of Heilongjiang Province, the Natural Science Foundation of Heilongjiang Province (E201436), the International Science and Technology Cooperation Program of China (2013DFR10630), and Specialized Research Fund for the Doctoral Program of Higher Education (SRFDP 20132302110031).

Received: May 5, 2015
Revised: May 18, 2015
Published online: July 14, 2015

[1] V. K. Thakur, G. Q. Ding, J. Ma, P. S. Lee, X. H. Lu, *Adv. Mater.* **2012**, *24*, 4071.
[2] G. A. Niklasson, C. G. Granqvist, *J. Mater. Chem.* **2007**, *17*, 127.
[3] C. G. Granqvist, *Sol. Energy Mater. Sol. Cells* **2012**, *99*, 1.
[4] T. Brezesinski, D. F. Rohlfing, S. Sallard, M. Antonietti, B. M. Smarsly, *Small* **2006**, *2*, 1203.
[5] A. Ghicov, S. P. Albu, J. M. Macak, P. Schmuki, *Small* **2008**, *4*, 1063.
[6] L. Guo, Y. Ren, J. Liu, S. Y. Chiam, W. K. Chim, *Small* **2014**, *10*, 2611.
[7] J. Scarminio, A. Lourenco, A. Gorenstein, *Thin Solid Films* **1997**, *302*, 66.
[8] K. Nagase, Y. Shimizu, N. Miura, N. Yamazoe, *Appl. Phys. Lett.* **1992**, *60*, 802.
[9] M. R. J. Scherer, L. Li, P. M. S. Cunha, O. A. Scherman, U. Steiner, *Adv. Mater.* **2012**, *24*, 1217.
[10] Y. Yang, D. Kim, P. Schmuki, *Electrochem. Commun.* **2011**, *13*, 1021.
[11] N. A. Chernova, M. Roppolo, A. C. Dillon, M. S. Whittingham, *J. Mater. Chem.* **2009**, *19*, 2526.
[12] E. Portiron, A. L. Salle, A. Varbaere, Y. Piffard, D. Guyomard, *Electrochim. Acta* **1999**, *45*, 197.
[13] J. M. McGraw, C. S. Bahn, P. A. Parilla, J. D. Perkins, D. W. Readey, D. S. Ginley, *Electrochim. Acta* **1999**, *45*, 187.
[14] Z. Q. Tong, J. Hao, K. Zhang, J. P. Zhao, B.-L. Su, Y. Li, *J. Mater. Chem. C* **2014**, *2*, 3651.
[15] L. Li, U. Steiner, S. Mahajan, *J. Mater. Chem.* **2010**, *20*, 7131.
[16] Y. Wang, K. Takahashi, K. Lee, G. Z. Cao, *Adv. Funct. Mater.* **2006**, *16*, 1133.
[17] B. L. Ellis, P. Knauth, T. Djenizian, *Adv. Mater.* **2014**, *26*, 3368.
[18] W. B. Kang, C. Y. Yan, X. Wang, C. Y. Foo, A. W. M. Tan, K. J. Z. Chee, P. S. Lee, *J. Mater. Chem. C* **2014**, *2*, 4727.

 © 2015 WILEY-VCH Verlag GmbH & Co. KGaA, Weinheim

[19] C. R. Xiong, A. E. Aliev, B. Gnade, K. J. Balkus, *ACS Nano* **2008**, *2*, 293.
[20] K. C. Cheng, F. R. Chen, J. J. Kai, *Sol. Energy Mater. Sol. Cells* **2006**, *90*, 1156.
[21] C. K. Chan, H. L. Peng, R. D. Twesten, K. Jarausch, X. F. Zhang, Y. Cui, *Nano Lett.* **2007**, *7*, 490.
[22] J. M. Velazquez, S. Banerjee, *Small* **2009**, *5*, 1025.
[23] K. Takahashi, Y. Wang, G. Z. Cao, *Appl. Phys. Lett.* **2005**, *86*, 053102.
[24] Y. Wang, H. M. Shang, T. Chou, G. Z. Cao, *J. Phys. Chem. B* **2005**, *109*, 11361.
[25] K. Honma, M. Yoshinaka, K. Hirota, O. Yamaguchi, *Mater. Res. Bull.* **1996**, *31*, 531.
[26] A. Benayada, H. Martinez, A. Gies, B. Pecquenard, A. Levasseur, D. Gonbeau, *J. Electron Spectrosc. Relat. Phenom.* **2006**, *150*, 1.
[27] J. Mendialdua, R. Casanova, Y. Barbaux, *J. Electron Spectrosc. Relat. Phenom.* **1995**, *71*, 249.
[28] G. Silversmit, D. Depla, H. Poelman, G. B. Marin, R. D. Gryse, *J. Electron Spectrosc. Relat. Phenom.* **2004**, *135*, 167.
[29] D. C. Sayle, D. H. Gay, A. L. Rohl, C. R. A. Catlow, J. H. Harding, M. A. Perrin, P. Nortier, *J. Mater. Chem.* **1996**, *6*, 653.
[30] Y. Y. Liu, M. Clark, Q. F. Zhang, D. M. Yu, D. W. Liu, J. Liu, G. Z. Cao, *Adv. Energy Mater.* **2011**, *1*, 194.
[31] J. Scarminio, P. R. Catarini, A. Urbano, R. V. Gelamo, F. P. Rouxinolb, M. A. Bica de Moraes, *J. Braz. Chem. Soc.* **2008**, *19*, 788.
[32] Z. Q. Tong, H. W. Yang, N. Li, H. Y. Qu, X. Zhang, J. P. Zhao, Y. Li, *J. Mater. Chem. C* **2015**, *3*, 3159.
[33] E. Potiron, A. Le Gal La Salle, A. Verbaere, Y. Piffard, D. Guyomard, *Electrochim. Acta* **1999**, *45*, 197.

© 2015 WILEY-VCH Verlag GmbH & Co. KGaA, Weinheim